VARIATION LAW OF COAL PERMEABILITY UNDER CYCLIC LOADING AND UNLOADING

by

Jingna GUO[a,b], Jiangfeng LIU[a,b*], Qiang LI[a], Xu CHEN[a], Zhanqing CHEN[a], Bingxiang HUANG[c], and Shuliang CHEN[c]

[a] The State Key Laboratory for GeoMechanics and Deep Underground Engineering and Jiangsu Key Laboratory of Environmental Impact and Structural Safety in Engineering, China University of Mining and Technology, Xuzhou, China
[b] The State Key Laboratory of Oil and Gas Reservoir Geology and Exploitation, Southwest Petroleum University, Chengdu, Sichuan, China
[c] The State Key Laboratory of Coal Resources and Safe Mining, China University of Mining and Technology, China

Original scientific paper
https://doi.org/10.2298/TSCI180907215G

In the excavation process, the coal pillar will undergo shear failure due to repeated loading and unloading from mining stress. Meanwhile, plastic flow will occur after shear failure. The permeability change of the coal pillar under plastic flow is closely related to the loading path. Through a permeability test of the coal sample after shear yielding under cyclic loading and unloading conditions, the variation law of permeability of a coal seam under plastic flow was obtained. The results show that the permeability of the coal sample increases as the axial strain decreases during the unloading phase. During the loading phase, as the axial strain increases, the permeability of the coal sample decreases. Scanning electron microscope tests show that the crack opening is larger at lower confining pressures. As the confining pressure increases, the crack opening decreases and moves toward the middle of the sample.

Key words: *coal permeability, coal seam, loading path, plastic flow*

Introduction

In the process of coal seam excavation, it is necessary to set up different types of support and safety isolation coal pillars. As the coal pillar is subjected to repeated loading and unloading from mining stress [1-3], shear yielding will occur in part of the coal pillar, and plastic flow will occur after yielding. The permeability of a coal pillar in the plastic zone is related to its stress-strain state. However, the single value correspondence relationship between permeability and strain no longer exists. Therefore, it is of great significance to study the change law of permeability of coal samples under cyclic loading and unloading after failure to reveal the mechanism of mine water inrush.

The pore structure, microcracks and joints of coal pillars change when the stress state of coal pillars redistributes under an external disturbance. Correspondingly, the permeability of coal pillars also changes [4-6]. Many domestic and foreign scholars have carried out a series of studies on the evolution law of permeability during the deformation and failure process

* Corresponding author, e-mail: jeafliu@hotmail.com

of coal. Most of these studies have focused on the relationship between the permeability and stress-strain [7-11] and the relationship between permeability and porosity [12]. Some scholars have conducted a permeability test under a full stress-strain process and obtained the law of permeability evolution with axial stress, strain, [10, 11]. Some other scholars have studied the effect of confining pressure on permeability and established the relationship between confining pressure and permeability. In addition, it has been found that the permeability is more sensitive to confining pressure than axial stress [6].

In fact, the change in porous media permeability is essentially the result of changes in the pore structure within the material [13]. Some scholars have obtained the relationship between permeability and porosity through the permeability experiment under stress. The results indicate that the permeability is exponentially related to porosity. However, plastic flow during rock deformation was neglected. During the on-site construction process, excavation of the roadway and the secondary stress field are actually the process of repeated loading and unloading of the coal pillar. Coal is a kind of strain-softening material, and the permeability shows complex dynamic characteristics with the deformation of the coal sample. After entering the plastic state, the one-to-one correspondence between the stress component and the strain component of the coal disappears. As a result, the one-to-one correspondence between the permeability and the strain component is broken. After yielding, the plastic strain component of coal is much larger than the elastic strain component, and the strain component also depends on the loading path.

Materials and methods

Material properties

The coal samples of this test were selected from the Long-de mining area, Shanxi Province. The sample size is 50 mm × 100 mm. Mercury injection test results show that the initial porosity of the coal sample was 8.97%, and the initial permeability was 4.54 m^2 × 10-15 m^2. At the end of the percolation test, a small piece was taken from the standard sample for the SEM test.

Test method

The seepage testing system was composed of an axial loading system (MTS816), confining pressure system (oil pump), permeation loop (hydraulic pump) and permeation meter (homemade cylinder). Its main functions included: applying axial load to the rock sample, applying confining pressure to the rock sample, and applying pore pressure (osmotic pressure) to the upper and lower end faces of the rock sample. The system diagram is shown in fig. 1.

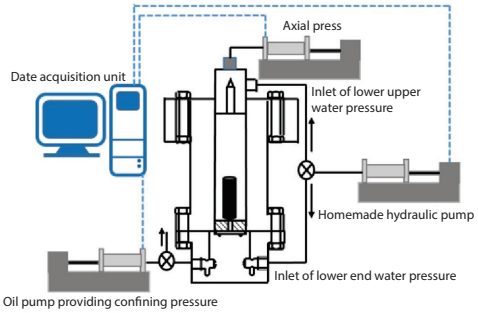

Figure 1. Schematic diagram of seepage testing system

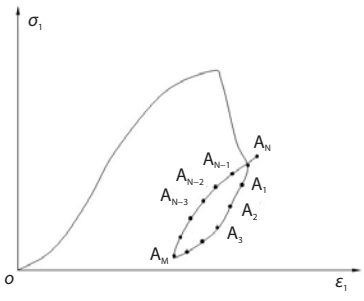

Figure 2. Insertion of penetration test points in test

In the plastic flow test with stress-strain hysteresis, the N points A_1, A_2, A_3,...A_N were set for the seepage tests, fig. 2, where A_i is the reverse point. The confining pressure was divided into four levels: 2.0 MPa, 4.0 MPa, 6.0 MPa, and 8.0 MPa. Each rock sample was loaded to the post-peak state A_M ($\sigma_1 = 0.7\ \sigma_1^{\max}$)

Failure criterion and water permeability

The purpose of the triaxial compression test was to determine the failure law of the rock and the basic mechanical parameters, such as cohesion and internal friction angle.

The damage of coal samples obeys the Mohr-Coulomb criterion [14]:

$$\frac{-\sigma_1 + \sigma_3 \tan^2(90° + \varphi)}{2} + \frac{2C\tan(90° + \varphi)}{2} \tag{1}$$

where C is the cohesion, and φ – the internal friction angle.

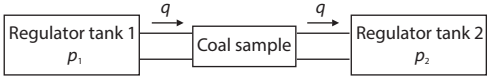

Figure 3. Principle of transient permeability testing system.

Due to the low permeability of coal, the transient method was used to determine the permeability of the coal sample. This principle is shown in fig. 3.

In fig. 3, both tanks had a volume of B and pressures of p_1 and p_2, respectively. The height and cross-sectional area of the rock samples are H and A, respectively. At the initial time, the pressure at both ends of the rock sample was p_{10} and p_{20} ($p_{10} > p_{20}$). The axial pressure gradient of the rock sample is $(p_{20} - p_{10})/H$. In the process of infiltration, the liquid in tank 1 entered tank 2 through the rock sample. As a result, the pressure of tank 1 kept decreasing, while that of tank 2 kept increasing, and the pressure gradient gradually decreased until the pressure of the two tanks reached an equilibrium state. Assume that the mass-flow rate of the liquid entering the rock sample of tank 1 is q. If the rock sample is water-saturated, the mass-flow rate of the liquid entering water tank 2 from the rock sample is q. The seepage velocity in the rock sample is $V = q/\rho A$. Water is compressible and has a compression factor:

$$\frac{1}{c_f} = \frac{\rho \mathrm{d}p_1}{\mathrm{d}\rho} \tag{2}$$

where c_f is the compressibility of water, and ρ – the density of water.

With the aid of the conditions $\mathrm{d}\rho = -q\mathrm{d}t/B$ and $q = \rho AV$, we have:

$$\frac{\mathrm{d}p_1}{\mathrm{d}t} = -\frac{AV}{c_f B} \tag{3}$$

Similarly:

$$\frac{\mathrm{d}p_2}{\mathrm{d}t} = -\frac{AV}{c_f B} \tag{4}$$

From eqs. (2) and (3) we give:

$$V = \frac{(c_f B)\mathrm{d}(p_1 - p_2)}{2A\mathrm{d}t} \tag{5}$$

According to Darcy's law, we get:

$$V = \frac{-k(p_2 - p_1)}{\mu H} \tag{6}$$

Substituting eq. (12) into eq. (13), we obtain:

$$\frac{\mathrm{d}(p_1 - p_2)}{p_1 - p_2} = \frac{-2Ak\mathrm{d}t}{c_f BH\mu} \tag{7}$$

During the test, the pressure data was collected at equal intervals, τ, and the total number of acquisitions was n. At the end of data collection, the pressure of the water tank at $t_f = \tau n$ was p_{1f} and p_{2f}, respectively. Integrating eq. (7), we obtain the following relationship:

$$k = \frac{c_f BH\mu[\ln(p_{10} - p_{20}) - \ln(p_{1f} - p_{2f})]}{2t_f A} \tag{8}$$

Results and analysis

Characteristics of coal sample failure

The results of the conventional triaxial compression test are shown in fig. 4 and tab. 1. The limit Mohr circle and its envelope line under various confining pressures are shown in fig. 5.

According to eq. (1), the yield condition of the aqueous coal samples:

$$-\sigma_1 + 6.45\sigma_3 + 34.31 = 0 \tag{9}$$

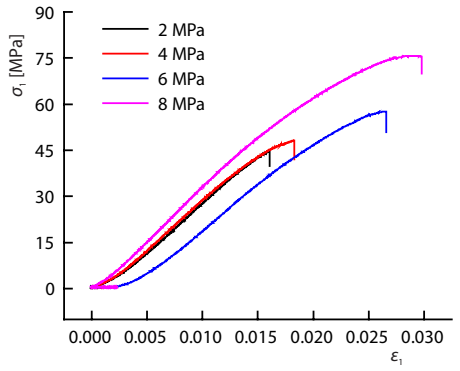

Figure 4. The $\varepsilon_1 - \sigma_1$ curves of the coal samples

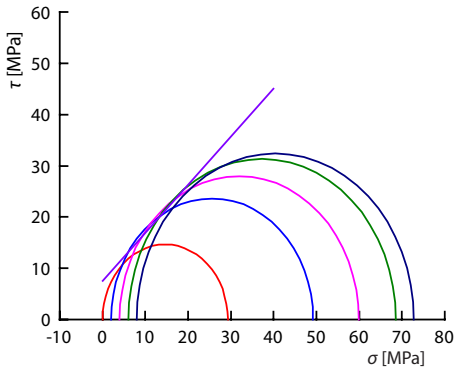

Figure 5. Limit Mohr circle of coal sample

Table 1. Peak stress, peak strain, internal friction angle, and cohesion of coal samples

Sample number	Diameter [mm]	Height [mm]	Confining pressure [MPa]	Peak stress [MPa]	Peak strain	Internal friction angle [°]	Cohesion [MPa]
L-2	49.8	99.9	2	44.66	0.0162	43.1	7.52
L-4	50.2	99.1	4	48.44	0.0198		
L-6	49.7	99.5	6	57.72	0.0275		
L-8	50.0	99.8	8	75.71	0.0301		

The angles between the line connecting the shear failure surface and the axis under different confining pressures are 9°, 14°, 22°, and 27°, respectively. The microstructure of the shear fracture surface of the coal sample was observed by SEM, fig. 6. Under low confining pressure, the macroscopic picture shows that the cracks penetrate up and down. Further, a microscopic observation of the local crack shows that the crack opening is large. As the confining pressure increases, the shear angle increases. The crack penetration position moves from the end of the sample to the middle. Further, it is found that the width of the main crack is reduced and the number of microcracks is increased.

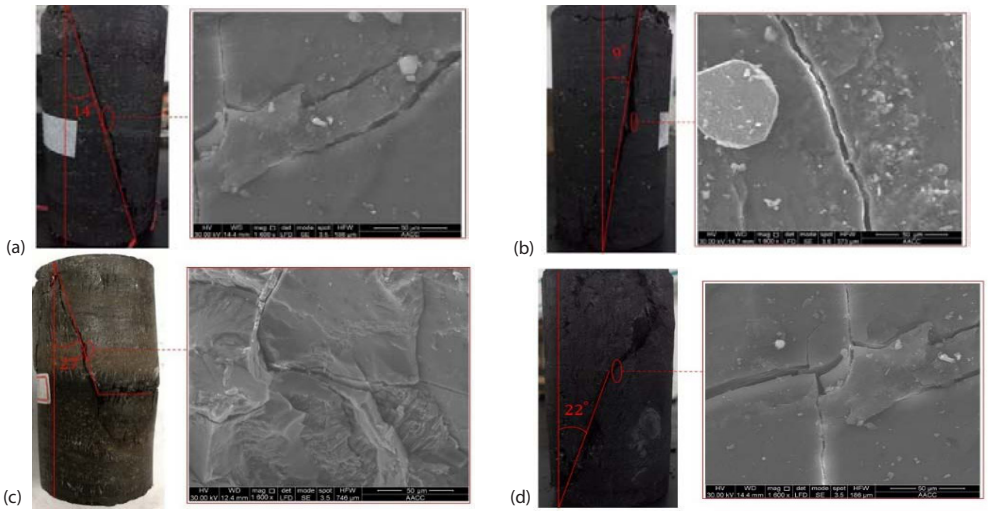

Figure 6. Microscopic view of the shear plane under different confining pressures; (a) σ_3 = 2 MPa, (b) σ_3 = 4 MPa, (c) σ_3 = 6 MPa, and (d) σ_3 = 8 MPa

Evolution of axial strain and permeability under cyclic loading and unloading

Under different confining pressures, the axial strain-permeability hysteresis curve was obtained in fig. 7.

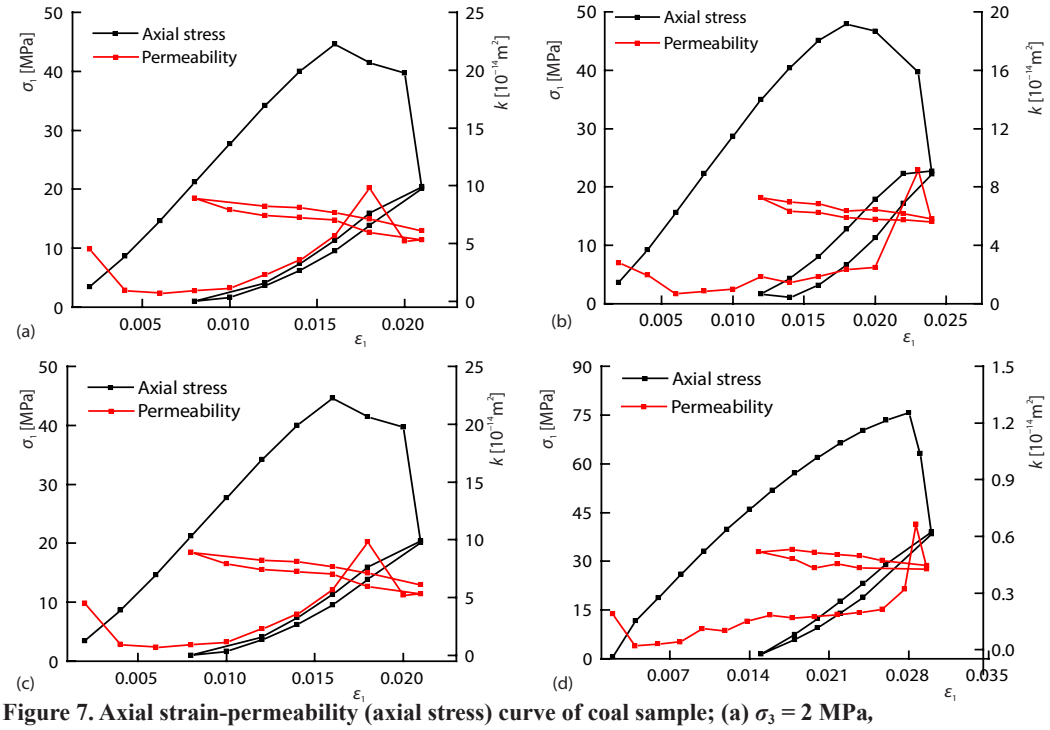

Figure 7. Axial strain-permeability (axial stress) curve of coal sample; (a) σ_3 = 2 MPa, (b) σ_3 = 4 MPa, (c) σ_3 = 6 MPa, and (d) σ_3 = 8 MPa

It can be seen from fig. 7 that that the permeability-axial strain evolution tendency of coal samples is quite close under different confining pressures. Taking the confining pressure of 4 MPa as an example, tab. 3 shows the variation of permeability with axial strain. In the pre-peak stage, when the axial strain increases from $\varepsilon_1 = 0.002$ to $\varepsilon_1 = 0.006$, the permeability decreases from $2.79 \cdot 10^{-14}$ m^2 to $6.56 \cdot 10^{-15}$ m^2. When the axial strain increases from $\varepsilon_1 = 0.006$ to the peak strain $\varepsilon_1 = 0.020$, the permeability increases from $6.56 \cdot 10^{-15}$ m^2 to $2.49 \cdot 10^{-14}$ m^2.

In the post-peak stage, when the axial strain increases from $\varepsilon_1 = 0.020$ to $\varepsilon_1 = 0.023$, the permeability increases from $2.49 \cdot 10^{-14}$ m^2 to a maximum of $9.16 \cdot 10^{-14}$ m^2. The peak permeability lags behind the stress peak. When the axial strain continues to increase from $\varepsilon_1 = 0.023$ to $\varepsilon_1 = 0.025$, the permeability decreases from $9.16 \cdot 10^{-14}$ m^2 to $5.61 \cdot 10^{-14}$ m^2 and tends to a stable value.

Table 3. Permeability at the inflection point of coal sample in $\sigma_3 = 4$ MPa

ε_1	k [m^2]	Remarks	Stage
0.002→0.006	$2.79 \cdot 10^{-14} \rightarrow 6.56 \cdot 10^{-15}$	$\varepsilon_1\uparrow, k\downarrow$	Elastic compaction
0.006→0.020	$6.56 \cdot 10^{-15} \rightarrow 2.49 \cdot 10^{-14}$	$\varepsilon_1\uparrow, k\uparrow$	Elastoplasticity
0.020→0.023	$2.49 \cdot 10^{-14} \rightarrow 9.16 \cdot 10^{-14}$	$\varepsilon_1\uparrow, k\uparrow$	Damage
0.023→0.025	$9.16 \cdot 10^{-14} \rightarrow 5.61 \cdot 10^{-14}$	$\varepsilon_1\uparrow, k\downarrow$	Post-peak residual
0.025→0.012	$5.61 \cdot 10^{-14} \rightarrow 7.27 \cdot 10^{-14}$	$\varepsilon_1\downarrow, k\uparrow$	Plastic unloading
0.012→0.025	$7.27 \cdot 10^{-14} \rightarrow 5.81 \cdot 10^{-14}$	$\varepsilon_1\uparrow, k\downarrow$	Plastic loading

Then, the test enters the unloading phase. When the axial strain is reduced from $\varepsilon_1 = 0.025$ to $\varepsilon_1 = 0.012$, the permeability increases from $5.61 \cdot 10^{-14}$ m^2 to $7.27 \cdot 10^{-14}$ m^2. Then, reverse loading is started. When the axial strain is increased from $\varepsilon_1 = 0.012$ to $\varepsilon_1 = 0.025$, the permeability is reduced from $7.27 \cdot 10^{-14}$ m^2 to $5.81 \cdot 10^{-14}$ m^2. In addition, the permeability in the reverse loading phase is greater than the permeability of the unloading section.

When the confining pressure is constant, the permeability decreases first and then increases during the axial loading process until the maximum value is reached after the failure. The maximum value of the permeability lags behind the stress peak. Throughout the testing process, the process of change in permeability can be divided into four phases. The first phase is the elastic phase. There are few primary microfractures, and the seepage mainly occurs through the pores of the sample. Due to compaction of the pores, the permeability is slightly reduced at this stage. The second stage is the elastoplastic stage. The primary and new fissures expand and penetrate, causing the seepage channel to gradually evolve from pores to pore-fractures. Therefore, the permeability coefficient increases slowly and then increases sharply. The third stage is the postfailure seepage stage. After reaching the peak, the permeability showed a gradual decline. The decrease in permeability is the result of recompacting after compression failure of the rock sample. The fourth stage is the cyclic loading and unloading stage. During the unloading phase, the permeability increases as the axial strain decreases. During the loading stage, the fracture is compacted with an increase in axial strain, which leads to a decrease in permeability. The permeability of the loading phase under the same axial strain is greater than that of the unloading phase, indicating that the coal sample produced irreversible deformation during the loading process. The strain-permeability curves of unloading and loading form a closed hysteresis. Moreover, the permeability-strain hysteresis loop corresponds to the closed hysteresis loop formed by the stress-strain curve and is *X* shaped. It shows that the change of permeability is closely related to the deformation damage of coal samples.

Conclusion

Through the seepage test of a damaged coal sample under loading and unloading conditions, The main conclusions:

- In the initial stage, with an increase in axial strain, the corresponding permeability decreases first and then increases until the coal sample is destroyed. The permeability reaches its maximum and lags behind the peak stress.
- During the unloading phase, the permeability of the coal increases with a decrease in axial strain.
- During the loading phase, the permeability of the coal decreases with an increase in axial strain. However, under the same axial strain, the permeability under loading is greater than that under unloading.
- The permeability hysteresis curve and its corresponding stress-strain hysteresis curve are in the shape of an *X*.

Acknowledgment

The authors are grateful to the support of the Fundamental Research Funds for the Central Universities (China University of Mining and Technology) (2017QNA29).

Nomenclature

A – rock sample area, [m^2]
B – water tank volume, [m^3]
C – cohesion, [MPa]
c_f – compression factor
d – diameter of rock sample, [mm]
H – height of rock samples, [mm]
k – permeability, [m^2]
p_1, p_2 – upper water pressure and lower water pressure, [MPa]
p_b – axial load, [kN]
q – flow, [m^{3}h^{-1}]
t_f – time to reach equilibrium, [s]
V – seepage velocity, [mms^{-}1]

Greek symbols

ε_1 – axial strain
μ – momentum viscosity of fluid, [N·sm^{-2}]
ρ – mass density of fluid, [kgm^{-3}]
σ_1, σ_3 – axial stress and confining pressure, [MPa]
σ_c – compressive strength, [MPa]
φ – internal friction angle, [°]

References

[1] Wu, G., *et al.,* Studying Unloading Failure Characteristics of a Rock Mass Using the Disturbed State Concept, *International Journal of Rock Mechanics and Mining Sciences, 41* (2004), 1, pp. 419-425
[2] Xie, H. Q., *et al.,* Study of The Unloading Characteristics of a Rock Mass Using the Triaxial Test and Damage Mechanics, *International Journal of Rock Mechanics and Mining Sciences, 41* (2004), 3, pp. 366-0
[3] He, M. C.,*et al.*, Rock Burst Process of Limestone and Its Acoustic Emission Characteristics Under True-Triaxial Unloading Conditions, *International Journal of Rock Mechanics and Mining Sciences, 47* (2010), 2, pp. 286-298
[4] Zheng, J., *et al.,* Relationships Between Permeability, Porosity and Effective Stress for Low-Permeability Sedimentary Rock, I*nternational Journal of Rock Mechanics and Mining Sciences, 78* (2015), Sept., pp. 304-318
[5] Zhang, Z., *et al.*, The Relationships Among Stress, Effective Porosity and Permeability of Coal Considering the Distribution of Natural Fractures: Theoretical and Experimental Analyses, *Environmental Earth Sciences, 73* (2015), 10, pp. 5997-6007
[6] Connell, L. D., *et al.*, An Analytical Coal Permeability Model For Tri-axial Strain and Stress Conditions, *International Journal of Coal Geology, 84* (2010), 2, pp. 103-114
[7] Mair, K., *et al.,* Influence of Confining Pressure On the Mechanical and Structural Evolution of Laboratory Deformation Bands, *Geophysical Research Letters, 29* (2002), 10, pp. 49-41
[8] Liu, J. F., *et al.,* Gas Permeability of a Compacted Bentonite–Sand Mixture: Coupled Effects of Water Content, Dry Density, and Confining Pressure, *Canadian Geotechnical Journal, 52* (2015), 1, pp. 1159-1167

[9] Liu, J. F., *et al.*, Experimental Research on Water Retention and Gas Permeability of Compacted Bentonite/Sand Mixtures, *Soils and Foundations, 54* (2014), 5, pp. 1027-1038
[10] Wang, J.A., *et al*., Fluid Permeability of Sedimentary Rocks in a Complete Stress–Strain Process, Engineering Geology, *63* (2002), 3-4, pp. 291-300
[11] Zhao, Y., *et al*., HydroMechanical Coupling Tests for Mechanical and Permeability Characteristics of Fractured Limestone in Complete Stress-Strain Process, *Environmental Earth Sciences*, *76* (2016), 1, pp. 24-42
[12] Zhang, Q., *et al*., Coupled Thermal-Gas-Mechanical (TGM) Model of Tight Sandstone Gas Wells, *Journal of Geophysics and Engineering*, *15* (2018), 4, pp. 1743-1752
[13] Liu, J. F., *et al*., Investigation into Water Retention and Gas Permeability of Opalinus Clay, *Environmental Earth Sciences*, *77* (2018), 5, pp. 5213-226
[14] Guo, J. N., *Experimental Study on Permeability Evolution of Coal Samples under Plastic Flow*, China University of Mining and Technology, Xuzhou, China, 2015

Paper submitted: September 7, 2018
Paper revised: December 12, 2018
Paper accepted: December 25, 2019